

Contents lists available at ScienceDirect

Talanta

journal homepage: www.elsevier.com/locate/talanta





Transferrin guided quasi-nanocuboid as tetra-enzymic mimics and biosensing applications

Qing Chen ^{a,1}, Bo Hu ^{d,1}, Dandan Zhang ^b, Qunxiang Ren ^a, Mengmeng Wang ^a, Peifeng Li ^c, Yang Zhang ^{a,*}

- ^a School of pharmacy, Shenyang Medical College, 146 Huanghe North Avenue, Shenyang 110034, China
- ^b School of Public Health, Shenyang Medical College, 146 Huanghe North Avenue, Shenyang 110034, China
- School of Basic Medicine, Shenyang Medical College, 146 Huanghe North Avenue, Shenyang 110034, China School of Basic Medicine, Shenyang Medical College, 146 Huanghe North Avenue, Shenyang 110034, China
- ^d Department of Biochemistry and Molecular Biology, School of Life Sciences, China Medical University, Shenyang 110122, China

ARTICLEINFO

Keywords: Manganese oxide Nanozymes Multi-enzyme mimics Colorimetric sensor Fluorimetric sensor

ABSTRACT

Given the promising prospect of nanozymes system with multi-enzyme mimetic activities, it is also a challenge for designing a controllable nanostructure as multi-enzymes mimics by protein-guided strategy. Here, transferrin (Trf)-directed manganese oxide with 3D nanomorphology was developed. Trf-Mn₃O₄ quasi-nanocuboids (NCs) was obtained by improved conditions for biomineralization, which employing Trf as biotemplate and Mn²⁺ as metal source in alkaline solution. Fortunately, not only was the controllable structure discovered, but Trf-Mn₃O₄ NCs also showed tetra-enzyme mimic activities involving peroxidase-, ascorbic acid oxidase-, catalase- and superoxide dismutase-mimic activities. Further, the catalytic properties and steady-state kinetic of Trf-Mn₃O₄ NCs was explored, systematically. Moreover, we develop simple colorimetric sensor based on the peroxidase-mimic activity of Trf-Mn₃O₄ NCs for the detection of gallic acid (GA) with the linear range within 0.1-40 µM, and the limit of detection was 41.2 nM (S/N = 3). Besides, a novel fluorimetric sensor for the detection of AA based on the ascorbic acid oxidase-mimic activity was proposed with the linear range of 0.5 μ M-10 μ M (R 2 = 0.9906) and 10 μ M-5 mM (R² = 0.9927), and LOD of 0.24 μ M (S/N = 3) was obtained. Both the proposed sensors showed outstanding detection performance, accuracy and repeatability, which realized the detection of GA and AA in real sample, respectively. The as-synthesized tetra-enzymic mimics not only enriched the species of nanozymes, particularly for the nanozymes with multi-enzyme mimic activities, the proposed sensors showed promising potential applications for biosensor in complex samples.

1. Introduction

Nanozymes are a series of nanomaterials with natural enzyme-mimic catalytic performance, which have attracted enormous research interests owing that overcome the shortcomings in comparison of natural enzymes in recent decade for their unique advantages of low cost, high stability, tunable size and catalytic activity, and ease of storge [1–3]. Since 2007, Yan and coworkers first reported magnetic Fe₃O₄ nanoparticles possessed intrinsic natural peroxidase-mimic property, which could catalyze the oxidation of the substrate 3,3',5,5'-tetramethyl benzidine (TMB) to produce a blue color reaction in the existence of H_2O_2 [4]. Inspired by this, various nanozymes were developed with natural enzymatic properties and exhibited tremendous achievements.

At present, the nanozymes have been reported mainly for carbon-based nanomaterials [5] and transition metal oxides [6–8], transition metal sulfides [9], and noble metals nanoparticles [10–13], which have been widely used in the fields of bio-detection [14], catalysts [15] and nanomedicine [16]. In addition, composite materials [17–19] and single-atom nanozyme [20–22] have been explored to improve enzyme-like activities of conventional nanozyme.

Although, a series of nanomaterials have been reported as a kind of inherent enzymic mimics, such as oxidase [23–25], peroxidase [26–28], catalase [29–31] or superoxide dismutase [8,32]. However, most of currently reported nanozymes showed single or double enzyme-mimic activities, significantly limiting their promising applications in biosensor and biomedicine [33–36]. Few works developed nanozyme

 $^{^{\}star}$ Corresponding author.

E-mail address: zhangyangpro@symc.edu.cn (Y. Zhang).

 $^{^{1}}$ Qing Chen and Bo Hu contributed equally to this work.

with multi-enzyme- mimic activities, and we really believed that nanozymes with multi-enzyme-mimic activities were prospected in wide range of applications [37,38]. Besides, the other intractable case in constructing nanozyme was that the substrate can directly and freely diffuse into the active sites, simultaneously, which leads a low selectivity. Namely, few enzyme mimics have been reported to conduct special catalytic reaction for their unique substrates, such as glutathione (GSH) [39], sarcosine [40], glucose [19,41] or ascorbic acid (AA) [42, 43] to realize selective determination. Generally, catalytic activity of nanozymes was related to the surface microenvironment involving active groups, hydrophilic and hydrophobic interactions, etc. To achieve a high activity in nanozyme, rational introduction and regulations of active sites and suitable architectures are one of challenges to be tackled. Given that, it becomes significance to explore enzymic mimics with multi-enzyme-like activities or a novel category of mimic enzymes.

In this work, we have developed transferrin guided quasinanocuboid nanozyme with multi-enzyme mimic activities for the first time, obtaining controllable morphology, satisfactory catalytic activity, high affinity and selectivity for its substrates in the directed design. In our case, we have demonstrated that Trf-Mn₃O₄ NCs with controllable morphology from 2D layer to 3D quasi-nanocuboid could be achieved by changing the synthesis conditions. As for another exciting result, not only did we explore multi-enzyme-like activities of Trf-Mn₃O₄ NCs, but also the peroxidase-minic (POD-mimic) and ascorbic acid oxidase-mimic (AAO-mimic) activities of Trf-Mn₃O₄ NCs could realize special catalysis for their unique substrates H₂O₂ and AA. We investigated systematically the effects of catalytic mechanism, steady-state kinetic and catalytic properities. Based on these findings, a sensitive colorimetric sensor for GA and a fluorimetric sensor for AA were developed. The proposed strategy exhibited high sensitivity and selectivity, low limit of detection, excellent accuracy and repeatability. Finally, the two as-proposed nanozyme-based sensors achieved the credible detection of GA and AA in real samples.

2. Experimental

2.1. Chemicals and apparatus

Transferrin (Trf), glutathione (GSH), L(+)-Cysteine (Cys) and terephthalic acid (TA) were purchased from Sigma-Aldrich. Ascorbic acid (AA), manganese chloride tetrahydrate (MnCl₂·4H₂O), sodium hydroxide (NaOH), hydrogen peroxide (H2O2, 30%), NaCl, KCl and CaCl2 were purchased from Sinopharm Chemical Reagent Co. Ltd. (Shanghai, China). O-phenylenediamine (OPD) was bought from J&K Scientific Ltd. 3,3,5,5-tetramethylbenzidine (TMB) and 3-(1,2-dihydroxyethyl) furo [3,4b]-quinoxaline (DFO) was purchased from TCI (Shanghai, China). DL-methionine (Met), serine (Ser), histidine (His), L-threonine (Thr), lysine (Lys), L-phenylalanine (Phe) and valine (Val) were obtained from Lanji Technology Development Co., Ltd. (Shanghai, China). Benzoic acid (Ba), salicylic acid (SA), p-hydroxybenzoic acid (p-HA), 3,4-dihydroxybenzoic acid (3,4-DA), 3,5-dihydroxy benzoic acid methyl ester (3,5-DA), 2,6-dihydroxybenzoic acid (2,6-DA), 2,4,6- trihydroxybenzoic acid (2,4,6-TA), 2,3,4-trihydroxybenzoic acid (2,3,4-TA) and gallic acid (GA) were purchased from Shanghai Maclean Biochemical Technology Co. Ltd. The ultrapure water (18.0 $\mbox{M}\Omega$ cm) was used throughout the whole experiment.

Transmission electron microscopy (TEM) images were recorded on a JEM-2100 F microscope (JEOL, Japan) operated at 200 kV. X-ray diffraction analysis was conducted with Cu $\rm K_{\alpha}$ radiation on Rigaku D/Max-2200 PC X-ray diffractometer. The hydrodynamic diameter was recorded using Zetasizer Nano-ZS instrument (Malvern, UK). The chemical composition was investigated using an ESCALab250 electron spectrometer (Thermo Scientific Corporation) with monochromatic 150 W Al $\rm K_{\alpha}$ radiations. The fluorescence analysis was performed on fluorescence spectrophoto meter F-7000 (Hitachi, Japan). The UV–Vis spectra and absorbance were measured by a Spark 10 M microplate

reader (Tecan, Switzerland) and spectrophotometer (U-2910, Hitachi, Japan). High performance liquid chromatography (HPLC) analysis was performed at ZQ 4000/2695 LC/MS with a 2966 diode array detector (Waters, USA).

2.2. Preparation of Trf-Mn₃O₄ NCs

Our investigation began with the synthesis of Trf-Mn $_3O_4$ NCs by controlled biomineralization method in alkaline solution containing Trf and Mn $^{2+}$. Briefly, 20 mg Trf was dissolved into MnCl $_2$ ·4H $_2O$ aqueous solution (10 mL, 6.35×10^{-3} M) under stirring for 30 min at room temperature, making sufficient interaction between Trf and Mn $^{2+}$. Then, the pH of the mixture solution was set to about 11 with NaOH solutions and kept stirring for 2 h until the mixture presenting the brown color. The products were dialyzed 48 h (MWCO 8000–14000) to eliminate extra ions and loose Trf. Finally, the products were centrifuged, freeze dried and stored at 4 °C.

2.3. Multi-enzyme mimic activities of Trf-Mn₃O₄ NCs

To investigate POD-mimic activity of Trf-Mn $_3O_4$ NCs, typical catalytic oxidation reaction was carried out in the presence of TMB and H $_2O_2$, TMB changed into oxidized TMB (oxTMB) to realize the color reaction. Briefly, the mixture of Trf-Mn $_3O_4$ NCs (50 μ g mL $^{-1}$), TMB (0.5 mM) and H $_2O_2$ (1 mM) added into acetate buffer (100 mM, pH 4.0), and incubated at 25 °C for 10 min. Then the characteristic absorbance of oxTMB ($\varepsilon_{650~nm}=39000~m^{-1}~cm^{-1}$) at 652 nm was recorded. We also investigated effects on the peroxidase-mimic activities involving pH (1–10) and temperature (25–75 °C) by above-mentioned assay. Three repetitious measurements were performed for every batch.

The ascorbic acid oxidase (AAO)-mimic activity was tested by adding AA (1 mM) to PBS solution (pH 8.0) with Trf-Mn $_3O_4$ NCs (100 μg mL $^{-1})$ and OPD (1 mM). After reacting for 5 min at 37 °C, the fluorescence spectra were recorded. In addition, optimal AAO-mimic activity was investigated by adjusting pH (4–10), temperature (25–60 °C) and incubation time (1–20 min) by above-mentioned assay.

To evaluate the CAT-mimic activity of Trf-Mn $_3$ O $_4$ NCs, generated oxygen (unit: mg L $^{-1}$) was tested at room temperature. Typically, 100 μ L Trf-Mn $_3$ O $_4$ NCs (2 mg mL $^{-1}$) and 200 μ L H $_2$ O $_2$ were added into buffer solution (pH 7.0), and the total volume of the mixture solution was 2 mL. The generated O $_2$ solubility was recorded at different times.

To evaluate superoxide dismutase (SOD)-mimic activity of Trf-Mn $_3$ O $_4$ NCs, a commercial colorimetric SOD assay kit (S311-10) was employed, and the assay was carried out strictly following to the instructions at room temperature. The SOD-mimic activities of Trf-Mn $_3$ O $_4$ NCs with different concentration was described as the inhibition ratio of competitive WST reaction with superoxide by natural SOD enzyme.

Steady-state kinetics analysis of nanozyme-mimic activities of Trf-Mn $_3$ O $_4$ NCs were performed by monitoring the changes of absorbance at 652 nm through adjusting the initial concentrations of the substrate TMB (0.1–3 mM) or H $_2$ O $_2$ (0.05–2 mM) at optimal conditions. The typical *Michaelis-Menten* curves were obtained, and *Michaelis* constant (K_m) and maximum velocity (V_{max}) were analyzed using the *Lineweaver-Burk* double reciprocal plot for inquiring the mechanism of proposed catalytic process of Trf-Mn $_3$ O $_4$ NCs. The kinetic parameters was determined by the equation $V = V_{max} * [S]/(K_m + [S])$, where V and V_{max} represented the reaction velocity and maximal reaction velocity, respectively. [S] was the concentration of substrate. K_m represented the *Michaelis* constant and indicated the affinity of the nanozyme for its substrate.

2.4. Colorimetric GA assay

Specific colorimetric GA assay of Trf-Mn₃O₄ NCs was conducted by adding 40 μ M GA and other antioxide interfering compounds (Na⁺, K⁺, Ca²⁺, Mn²⁺, Met, Ser, His, Thr, Val, Lys, Phe, GSH, AA, Cys) into acetate

Q. Chen et al. Talanta 240 (2022) 123138

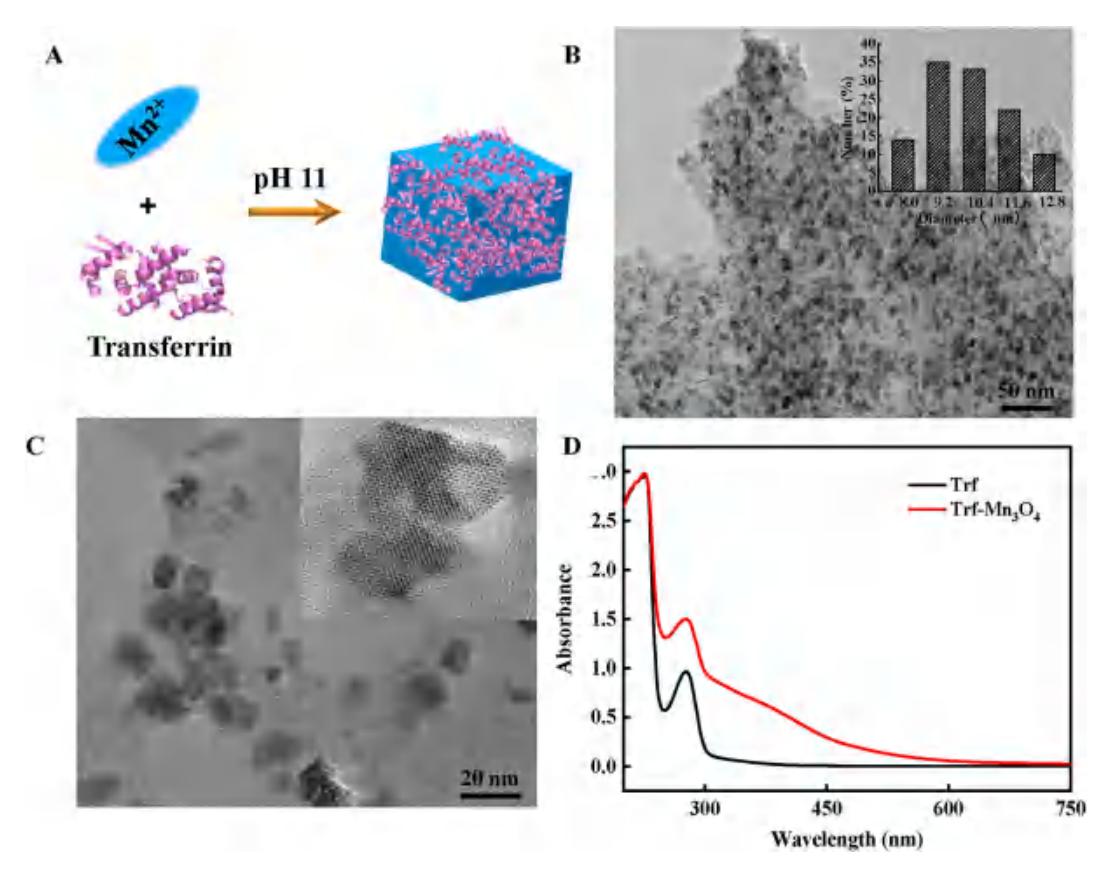


Fig. 1. Trf-directed synthesis and characterization of Trf-Mn₃O₄ NCs. (A) Synthesis schematic of Trf-Mn₃O₄ NCs. (B, C) TEM images of Trf-Mn₃O₄ NCs with the different magnification and particle size distribution diagram of Trf-Mn₃O₄ NCs (inset of B). (D) UV–Visible spectra of Trf and Trf-Mn₃O₄ NCs.

buffer solution (pH 4.0) containing Trf-Mn $_3$ O $_4$ NCs (50 μg mL $^{-1}$), TMB (2 mM) and H $_2$ O $_2$ (1 mM), incubated for 10 min at 30 °C. For further exploring the selectivity of the colorimetric GA assay, a comparison of antioxidant behavior of similar structure with GA, except for positions and numbers of hydroxyl involving GA, Ba, p-HA, SA, 3,4-DA, 3,5-DA, 2,6-DA, 2,4,6-TA, 2,3,4-TA were carried out in the same assay. The absorbance of oxTMB at 652 nm was measured.

2.5. Fluorimetric AA assay

Fluorimetric AA assay was performed by adding a series of concentrations of AA to the buffer solution (pH 8.0) with Trf-Mn $_3$ O $_4$ NCs (100 μg mL $^{-1}$) and OPD (1 mM), reacted at 37 °C for 15 min. The maximum fluorescence emission wavelength at 425 nm were recorded. For further exploring the selectivity of the fluorimetric AA assay, a series of interferents (ions, amino acids and others) were added into above mixture solution instead of AA. Finally, serum from healthy people was chosen as practical samples for detecting AA.

3. Results and discussion

3.1. Controllable synthesis of Trf-Mn₃O₄ NCs

Synthetic procedure of Trf-Mn $_3O_4$ NCs was presented in Fig. 1A. We first explored the preparation of Trf-Mn $_3O_4$ NCs, in which using Trf as template and Mn $^{2+}$ as metal source. Mn $^{2+}$ was oxidized and nucleated, then nuclei continued to grow gradually into Mn $_3O_4$ nanocrystals in the presence of Trf under alkaline reaction conditions. Trf severed as template and stabilizer, which provided the stable structure and enhanced the dispersion of obtained nanocrystals. To obtain 3D morphology, we tried to optimize the concentration ratio of Mn $^{2+}$ and Trf, and TEM and XRD were performed to indicate the morphology and the phase

composition of Trf-Mn₃O₄ NCs. As shown in Fig. 1B, the Trf-Mn₃O₄ NCs showed uniform quasi-nanocuboid with a small average size of 10.1 nm. The lattice presented in TEM (Fig. 1C) accorded with $d_{[101]} = 0.492$ nm, indicating highly crystalline nature of the as-prepared Trf-Mn₃O₄ NCs. When the mass ratio of Mn²⁺/Trf was lower (0.126/1), Trf-Mn₃O₄ crystals were unorganized cross-linked and tended to form primary lamellar network structure (Fig. S1A). With the increasing mass ratio of Mn^{2+}/Trf (0.315/1), the laminate morphology was gradually transforming and the significant edges were presented among the as-prepared Trf-Mn₃O₄ particles with larger size (about 40 nm) (Fig. S1B). When the mass ratio of Mn²⁺/Trf was increased to 0.63/1, the particle size was further reduced and quasi-nanocuboid of Trf-Mn₃O₄ NCs was formed (Fig. 1B and C). The AFM image illustrated that the thickness of Trf-Mn₃O₄ NCs was about 6.1 nm (Fig. S2). In view of this, the ratio of concentration for Mn²⁺/Trf could affect the growth of nanocrystals and made the Trf-Mn₃O₄ with controllable structure from 2D to 3D morphology. The protein-directed manganese oxide nanostructure have also been reported, however, manganese was beneficial to obtain the 2D lamellar nanostructures [44]. We successfully obtained 3D morphology of Trf-templated nanostructure through adjusting the synthesis conditions, breaking the common phenomenon. In this work, we selected as-prepared 3D Trf-Mn₃O₄ NCs for further studied. UV-Vis of Trf-Mn₃O₄ NCs (Fig. 1D) showed typical absorbance of Trf at 280 nm and manganese oxide at 372 nm. To evaluate secondary structure and the biological activity of Trf after producing Trf-Mn₃O₄ NCs, CD spectra were recorded for both Trf standard solution and Trf-Mn₃O₄ NCs in a same solution. CD spectra illustrated negative absorptions of predominant $\alpha\text{-helical}$ and β-sheet structure in the far UV region at 208 nm, 216 nm and 220 nm for Trf standard. A similar CD spectrum was discovered for Trf-Mn₃O₄ NCs, indicating the maintenance of its primary secondary structure (Fig. S3).

XRD pattern of Trf- Mn_3O_4 NCs was shown in Fig. S4. All the measured diffraction peaks were well matched to the crystal faces of (1

Q. Chen et al. Talanta 240 (2022) 123138

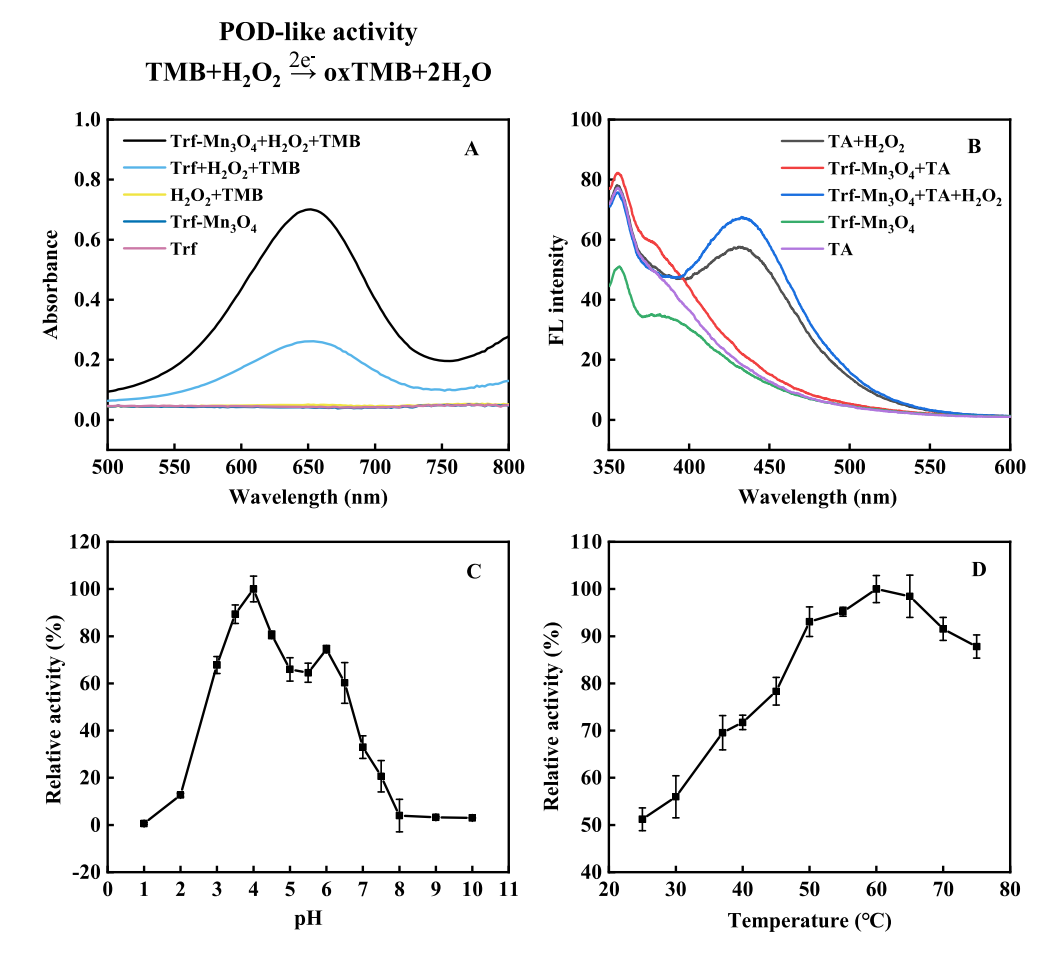


Fig. 2. POD-mimic activity of Trf-Mn $_3O_4$ NCs. (A) Typical absorption spectra of TMB, oxidation catalyzed by Trf-Mn $_3O_4$ NCs and control groups in the presence of H_2O_2 at pH 4.0. (B) Free radical capture experiment by TA and control groups. pH (C) and temperature-dependent (D) on POD-mimic activity of the Trf-Mn $_3O_4$ NCs. Error bars represented the standard error derived from three repetitive measurements.

0 1) (1 0 3), (2 1 1) and (2 2 4) of Mn_3O_4 from standard spectrum (JCPDS No. 97-064-3199), demonstrating their highly crystalline nature. X-ray photoelectron spectroscopy (XPS) was executed to demonstrate the chemical valence and binding of the element. In the full-survey-scan XPS spectrum of Trf-Mn₃O₄ NCs (Fig. S5A), C, N, O, S and Mn elements coexisted in the hybrid. The high-resolution Mn 2p spectrum (Fig. S5B) exhibited a notable peak with binding energies at 640.7 eV for Mn 2p3/2 in good agreement with reported Mn^{II} cations, typical peaks at 642.3 and 655.2 eV resulted from MnIII cations, indicating the presence of Mn₃O₄ in the composite [45,46]. In addition, three characteristic peaks around at 533.65, 532.75, 531.55 eV for O 1s (Fig. S5C), which are ascribed to O-H, Mn-O and C=O groups. The C 1s involves four peaks respectively centered at 288.15, 286.45, 285.65 and 284.55 eV, which are correspond to C=O, C-O, C-N, and C=C groups (Fig. S5D). Whereas, the N 1s and S 2p both appear distinct bulge peaks, which completely originates from Trf (Figs. S5E and F).

3.2. To explore the tetra-enzyme-mimic activities of Trf-Mn₃O₄ NCs

We explored whether Trf- Mn_3O_4 NCs have enzyme-mimic activities using suitable substrates for natural enzymes. First, we evaluated peroxidase-mimic activity of Trf- Mn_3O_4 NCs, which reduces H_2O_2 , generating free radicals. In detail, TMB as model indicator used in a H_2O_2 -mediated reaction, which could be oxidated to oxTMB and presented the strong absorbance at 652 nm.

Typical visible spectra was presented at 652 nm for the mixture of TMB/Trf- Mn_3O_4 NCs/ H_2O_2 (Fig. 2A) and the intensity increased with the concentration of Trf- Mn_3O_4 NCs (Fig. S6), resulting in the formation

of oxTMB by $\rm H_2O_2$ in the presence of Trf-Mn₃O₄ NCs. Meanwhile, similar absorption with lower intensity was found in the presence of TMB/Trf/H₂O₂, except that, no similar results presented for other control groups. Therefore, it proved that the synthesized Trf-Mn₃O₄ NCs possessed POD-like activity, and the properties provided by the Trf itself and formed unit of Mn₃O₄ NCs.

In addition, TA as capturer, used to catch free radicals produced from this catalytic oxidation process and synthesized 2-hydroxyterephthalic acid, which showed obvious fluorescence peak at 435 nm (Fig. 2B). The results declared the Trf-Mn $_3$ O $_4$ NCs had the feature of prompt the decomposition of hydrogen peroxide to produce free radicals and revealed the POD-mimic activity of Trf-Mn $_3$ O $_4$ NCs. Moreover, the POD-mimic activity of Trf-Mn $_3$ O $_4$ NCs presented pH- and temperature-dependence, and the highest catalytic activity was obtained at pH 4.0 and 60 °C (Fig. 2C and D), which was similar to natural peroxidase.

To understand the peroxidase-mimic activity of Trf-Mn₃O₄ NCs, the apparent steady-state kinetics were investigated under the optimal conditions. Accordingly, the catalytic reaction speeds for Trf-Mn₃O₄ NCs (Figs. S7A and S7B) increased with the substrate concentrations increasing gradually until up to a plateau, demonstrating the catalytic reaction followed the *Michaelis-Menten* kinetics. The kinetic parameters $K_{\rm m}$ and $V_{\rm max}$ were calculated respectively by *Lineweaver–Burk* equation. As for TMB, the $V_{\rm max}$ was 5.38 μ M min⁻¹ and Km was 0.49 mM (R² = 0.998) (Fig. S8A). In addition, the $V_{\rm max}$ and $K_{\rm m}$ for H₂O₂ were calculated to be 4.53 μ M min⁻¹ and 0.03 mM, respectively (Fig. S8B). Those higher $V_{\rm max}$ values proved the satisfactory POD-like catalytic activity of Trf-Mn₃O₄ NCs. Moreover, it clearly showed all lines have the same slope and preserve the parallel relationship with each other, as fixed the one

Q. Chen et al. Talanta 240 (2022) 123138

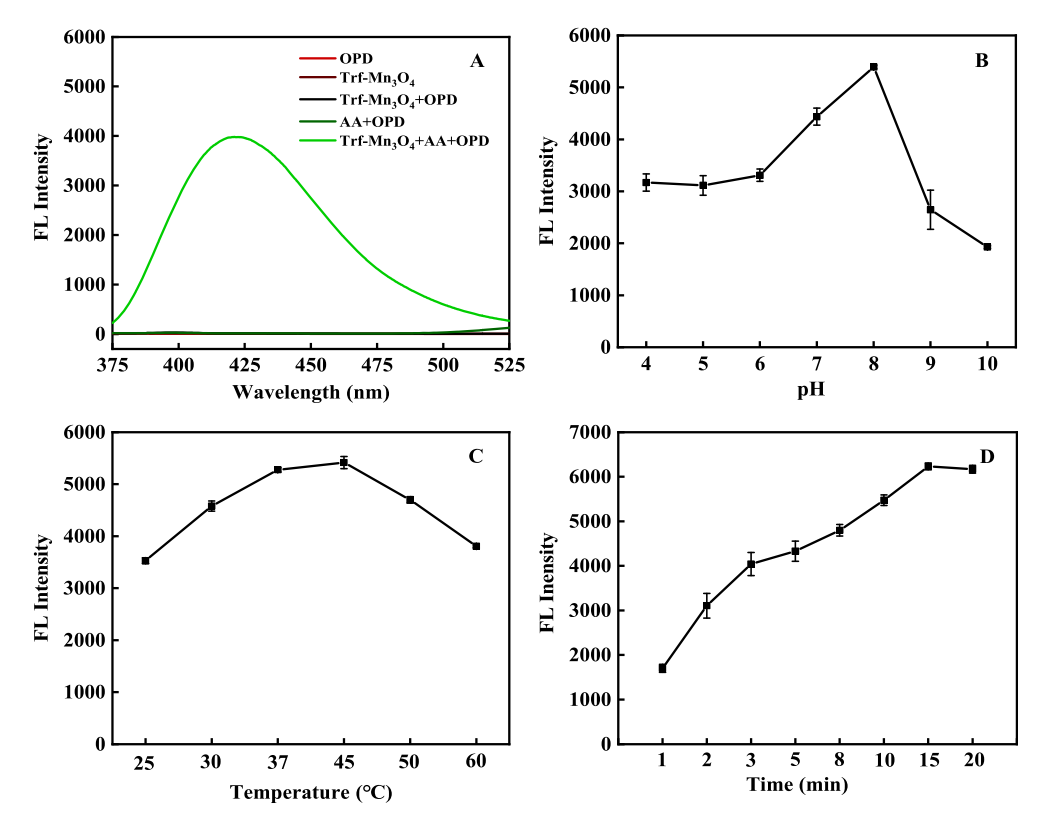


Fig. 3. AAO-mimicking activity (A), and effect of pH (B), temperature (C) and reaction time (D) on the AAO-mimic activity of Trf-Mn₃O₄ NCs.

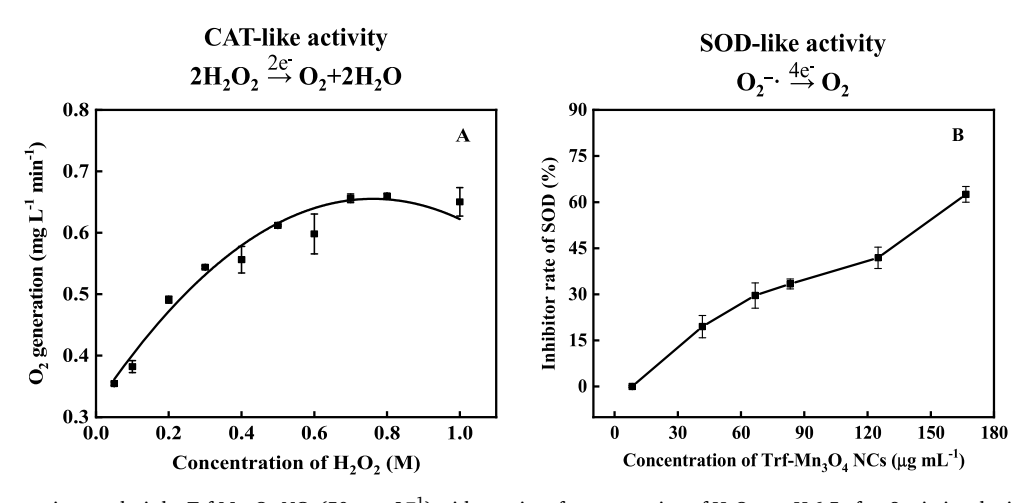


Fig. 4. (A) Oxygen generation catalysis by $Trf-Mn_3O_4$ NCs (50 μg mL⁻¹) with a series of concentration of H_2O_2 at pH 6.5 after 8 min incubation. (B) Inhibitor rate of SOD on a series of concentration of $Trf-Mn_3O_4$ NCs at pH 8.0.

substrate (TMB or H_2O_2) concentration (Figs. S7C and S7D), which illustrated the result consistent with Ping-Pong BiBi mechanism, which formed a peroxide radical intermediate in the process of catalyzing H_2O_2 in order to oxidize TMB.

In order to evaluate the AAO-mimic activity of Trf-Mn $_3$ O $_4$ NCs, a fluorescent system was constructed. In this detection system, AA could be catalytic oxidized to DHAA in the presence of AAO and DHAA continued to react with OPD to generate fluorescigenic DFQ, emitting strong fluorescence at 425 nm (Fig. 3A). Then we studied the effect of pH, temperature and time on AAO-mimic activity. As results, Trf-Mn $_3$ O $_4$ NCs showed maximum AAO-mimic activity at weakly alkaline pH 8.0 and maintained more than 90% activity in pH range from 7.0 to 8.3 (Fig. 3B). Afterwards, optimum reaction temperature and time were determined, and the optimized temperature range was 45 °C (Fig. 3C)

and time was 15 min (Fig. 3D).

Inspire by catalase could catalyze H_2O_2 to decompose to generate O_2 , to test if Trf-Mn₃O₄ NCs possess CAT-mimic activity, we used a dissolved oxygen meter to monitor O_2 generation with a series of concentration of H_2O_2 (Fig. 4A) at an optimal pH (pH = 6.5) (Fig. S9A) and reaction time (Fig. S9B). These results provided direct evidence that proposed Trf-Mn₃O₄ NCs possessed CAT-mimic activity.

We chose a commercialized SOD-assay to test whether Trf-Mn $_3$ O $_4$ NCs had SOD-mimic activity. In the method, water-soluble WST-1 react with superoxide anion radicals ($O_2^{\bullet -}$) to generated a kind of dye (WST-1 formazan), then the reaction process was inhibited by the SOD or the analogue with SOD-mimicking activity. Herein, the SOD-mimic properties of a series of concentrations of Trf-Mn $_3$ O $_4$ NCs was tested as the percentage inhibition of the competitive WST reaction with $O_2^{\bullet -}$ by

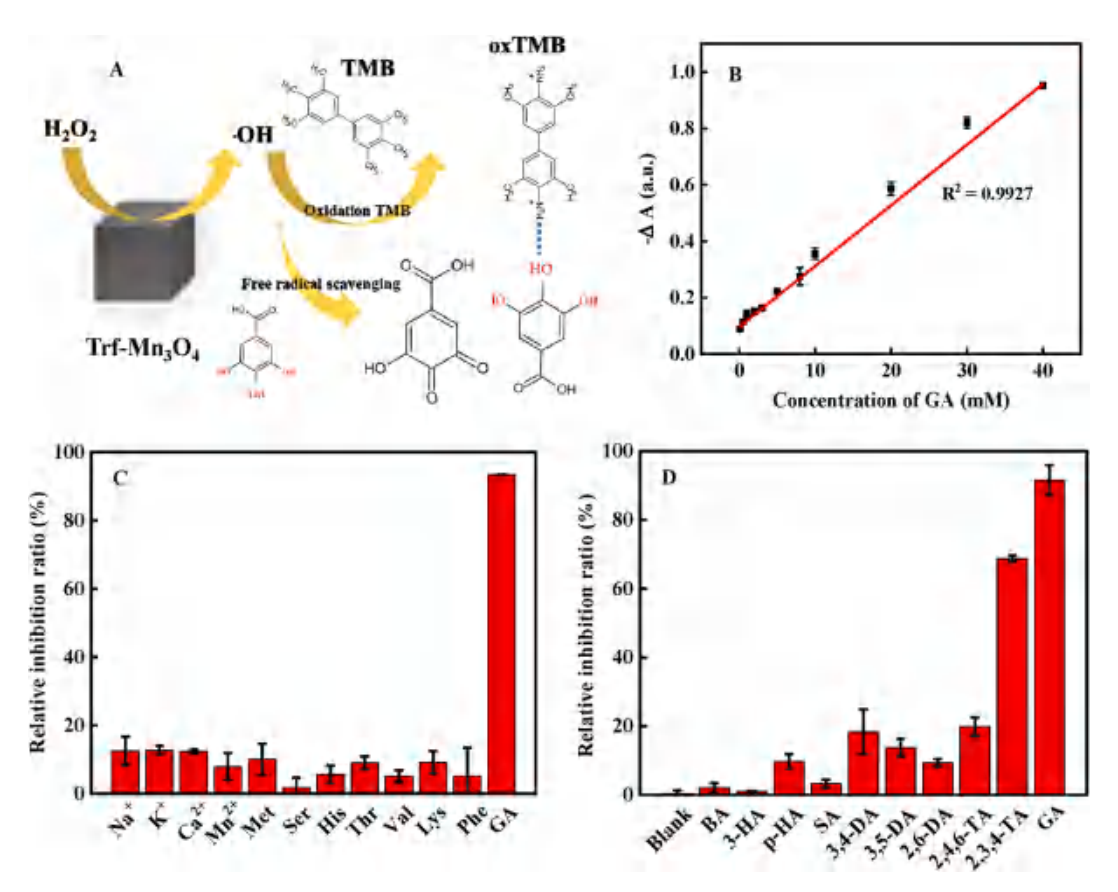


Fig. 5. (A) Reaction mechanism illustrate of selectively detect GA. (B) The calibration curve corresponding to GA concentration in the range of 0.1–40 μM. (C) Different substrates including conventional ions and amino acids induced inhibition ratio. (D) Determination of the active site of gallic acid compared with different hydroxyl compounds. Error bars represent the standard deviations detected for three repetitive measurements.

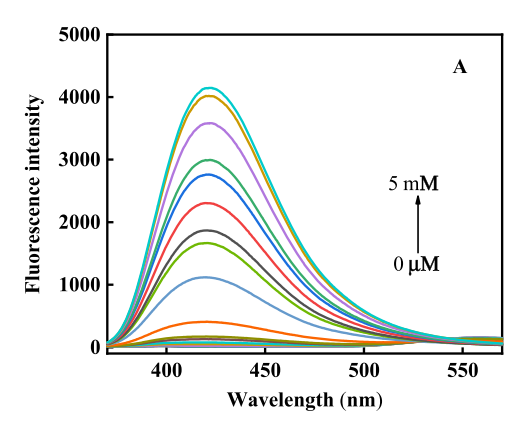
natural SOD enzyme. As shown in Fig. 4B, a palpable inhibitory effect was exhibited with increased concentration of Trf-Mn $_3$ O $_4$ NCs, indicating the SOD-mimic activity. Taken together, these results provided credible evidence that as-prepared Trf-Mn $_3$ O $_4$ NCs possess four enzymemimicking activities including POD, AAO, CAT and SOD, which could as potential enzyme mimics for many fields.

3.3. Colorimetric sensing GA

GA, a strong antioxidant, which was considered to reduce the blue color of oxTMB until colorless because of its reducibility (Fig. 5A). Specific colorimetric assay for GA was performed in the presence of TMB/H₂O₂ by using POD-like activity of Trf-Mn₃O₄ NCs under the optimal conditions. As shown in Fig. 5B, different concentrations of GA was added the mixture which given rise to fading of blue color, and the decreased UV-vis absorption spectra at 652 nm ($\Delta A = (A_0-A)/A_0$) was rising with the GA concentration increased. A good linear relationship between GA concentration and absorbance at 652 nm with a wide range (0.1–40 μ M), the linear regression equation was y=0.0223~x+0.1083 $(R^2 = 0.9927)$ and the limit of detection (LOD) was 41.2 nM (S/N = 3). Compared with other GA assay methods including some electrochemical methods, our nanozyme-based colorimetric assay exhibited the lowest LOD (Table S1). Then, we studied the selectivity of proposed GA assay methods by examining possible interfering substances including ions and conventional amino acids, on GA detection under the same reaction conditions. Fig. 5C showed that the inhibition ratios for both 100-fold excess ions and amino acids were less than 20% in the system.

For further investigated possible mechanism, we hypothesized that the existent antioxidant behaviors mainly caused by active three phenolic hydroxyl groups of GA, and could participate in clear away free radicals or active oxygen species, prevented TMB from being oxidized. Thereby, the antioxidant behavior was examined between GA and other similar structures with different positions and numbers of hydroxyl involving Ba, p-HA, SA, 3,4-DA, 3,5-DA, 2,6-DA, 2,4,6-TA, 2,3,4-TA, GA (40 µM) in the same conditions. As shown in Fig. 5D, the results presented certain regularity, less than 20% inhibition ratio was obtained for other similar structures except 2,3,4-TA, and the inhibition ratio gradually enhanced with hydroxyl number increased. 2,3,4-TA showed a relative high inhibition ratio (68.73%), but lower than GA (91.55%). These demonstrated that p-hydroxy and m-hydroxy were easier to achieve the reduction of oxTMB and the hydroxy group at the para position of the carbonyl group was the active center, which was more likely to gain electrons and be oxidized.

We detected GA in real in red drinks and green drinks by proposed sensor system through the standard addition method. On basis of the calibration curve, the GA concentrations were calculated be 6.28 and 7.99 M for red tea drink and green tea drink, respectively. As shown in Table S2, the detected GA concentrations according with their given concentrations. Different concentrations GA were added into the diluted sample solutions, the results of a series of experiments indicated the relative standard deviation (RSD) were within 0.15-0.70% and the average recoveries within 101.2-102.8%, indicating the GA detection method based on the Trf-Mn₃O₄ NCs possessed the accuracy and repeatability. In addition, the testing consistency evaluation between this method and the testing standard protocol of RP-HPLC has been conducted in red drinks and green drinks, respectively. As shown in Table S3, It can be seen that the proposed method can accurately detect GA in actual samples with satisfactory reproducibility and consistent with the standard method.



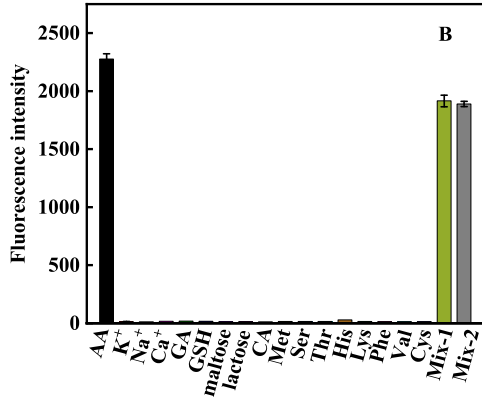


Fig. 6. (A) Fluorescence spectra of mixture of OPD/AA/Trf- Mn_3O_4 NCs varying with AA concentrations (0–100 μ M). (B) Selectivity determination of fluorimetric AA sensor. AA was at a concentration of 1 mM, other interferents were 1 mM. Mix-1: mixture except amino acids, Mix-2: a mixture of all of the above.

3.4. Fluorimetric sensing AA

The AAO could catalytic oxidized AA to DHAA, and DHAA further reacted with OPD to produce fluorescent product DFQ (3-(1,2-dihydroxyethyl)furo[3,4b]- quinoxaline) with emission wavelength 425 nm. Inspired by this principle, we proposed a novel fluorescence sensor for determination of AA based on the AAO-mimic activity of Trf-Mn₃O₄ NCs by elucidating the relationship between AA concentration and the fluorescence strength at emission wavelength 425 nm (Fig. 6A). The linear calibration ranges were obtained within 0.5 μM -10 μM and 10 μ M-5 mM, with regression equations of F = 31.227C - 29.227 (R2 = 0.9906) and F = 415.81C - 211.68 ($R^2 = 0.9927$) (Fig. S10), and the limit of detection was 0.24 μM AA (S/N = 3) for the proposed nanosensor. The antijamming capability of the proposed sensor was evaluated by analyzing some potential interferences involving of conventional ions, amino acids, lactose, maltose and antioxidants. As results in Fig. 6B, there was no obvious interference signal for other species tested whether individual substances or mixtures, indicating that the sensor based on Trf-Mn₃O₄ NCs possessed good selectivity for AA detection.

To verify the practicability of proposed nanosensor for real sample, we detected AA from the normal human serum. The AA concentrations we detected according with normal range of indicators for healthy people. Besides, recovery experiments were carried out by adding a series of concentrations of AA solution. As results in Table S4, the average recovery of all the samples was range from 95.3% to 102.5%, and the RSD was lower than 5.0%, indicating that the proposed sensor was reliable and could apply to detect AA in real sample. For further demonstrating the testing consistency, the comparaing with correlative criterion (RP-HPLC) was performed in the same human serum. Similar and satisfactory results were obtained (Table S5), proving the accuracy and applicability of the proposed method.

3.5. The stability and reliability of the nanozyme mimic activity

The Trf- Mn_3O_4 NCs nanozyme has high stability and no obvious aggregation in aqueous solution after 30 days (Fig. S11), and the corresponding POD-like and AAO-like activities were determined. We found that the POD-like still kept over 85% and AAO-like activities of Trf- Mn_3O_4 NCs maintained over 90%, elucidating the outstanding stability and reliability of Trf- Mn_3O_4 NCs nanozyme.

4. Conclusions

In summary, we have reported for the first time that a single quasinanocuboid, a smart Trf-Mn₃O₄ NCs, exhibited multi-enzyme mimetic activities involving POD-, AAO-, CAT- and SOD-mimic activities. We demonstrated that Trf-Mn₃O₄ NCs with controllable morphology could be achieved by adjusting the synthesis condition. The mechanisms and kinetics of POD- and AAO-like activities of Trf-Mn₃O₄ NCs were investigated. Further, the Trf-Mn₃O₄ NCs as peroxidase mimetics provided a colorimetric assay for GA with a wide linear range from 0.1 μM to 40 μM . Similarly, we utilized the Trf-Mn₃O₄ NCs as ascorbic acid oxidase mimics to design a fluorimetric sensor for AA, and the sensor developed exhibited sensitive and selective detection of AA with a wide linear range from $0.5~\mu M$ to $10~\mu M$ and $10~\mu M$ to 5~m M, the LOD was $0.24~\mu M$. We presented both colorimetric detection of GA and fluorimetric detection of AA, obtaining high sensitivity, low LOD, outstanding stability and reliability for application in real samples. This work provided a new avenue for the protein-directed synthesis nanozyme and a new species of manganic oxide-based nanozyme. More significantly, the Trf-Mn₃O₄ NCs nanozyme with multi-enzyme mimetic activities have a promising potential for other biosensors, biocatalysis and biomedicine.

Credit author statement

Qing Chen: Validation, Writing-review and editing, Funding acquisition. Bo Hu: Writing-review and editing, Software, Investigation. Dandan Zhang: Investigation. Qunxiang Ren: Supervision, Investigation. Mengmeng Wang: Investigation. Peifeng Li: Investigation, Writing-review and editing. Yang Zhang: Conceptualization, Methodology, Investigation, Writing-original draft, Project administration, Funding acquisition.

Declaration of competing interest

The authors declare that they have no known competing financial interests or personal relationships that could have appeared to influence the work reported in this paper.

Acknowledgments

The authors appreciate financial support from Postdoctoral Science Foundation of China (2018M642615), National Natural Science Foundation of China (No. 21804093) and Natural Science Foundation of Shandong Province (ZR2017BB053).

Appendix A. Supplementary data

Supplementary data to this article can be found online at https://doi.org/10.1016/j.talanta.2021.123138.

References

- [1] J.X. Wu, X.Y. Wang, Q. Wang, Z.P. Lou, S.R. Li, Y.Y. Zhu, L. Qin, H. Wei, Nanomaterials with enzyme-like characteristics (nanozymes): next-generation artificial enzymes (II), Chem. Soc. Rev. 48 (2019) 1004–1076.
- [2] Y.Y. Huang, J.S. Ren, X.G. Qu, Nanozymes: classification, catalytic mechanisms, activity regulation, and applications, Chem. Rev. 119 (2019) 4357–4412.
- [3] L.Z. Gao, X.Y. Yan, Discovery and current application of nanozyme, Prog. Biochem. Biophys. 40 (2013) 892–902.
- [4] L.Z. Gao, J. Zhuang, L. Nie, J.B. Zhang, Y. Zhang, N. Gu, T.H. Wang, J. Feng, D. L. Yang, S. Perrett, X.Y. Yan, Intrinsic peroxidase-like activity of ferromagnetic nanoparticles, Nat. Nanotechnol. 2 (2007) 577–583.
- [5] S. Wang, R. Cazelles, W.C. Liao, M. Vazquez-Gonzalez, A. Zoabi, R. Abu-Reziq, I. Willner, Mimicking horseradish peroxidase and NADH peroxidase by heterogeneous Cu²⁺-modified graphene oxide nanoparticles, Nano Lett. 17 (2017) 2043–2048.
- [6] S.Y. Fu, S. Wang, X.D. Zhang, A.H. Qi, Z.R. Liu, X. Yu, C.F. Chen, L.L. Li, Structural effect of Fe₃O₄ nanoparticles on peroxidase-like activity for cancer therapy, Colloids Surf., B 154 (2017) 239–245.
- [7] H.M. Jia, D.F. Yang, X.N. Han, J.H. Cai, H.Y. Liu, W.W. He, Peroxidase-like activity of the Co₃O₄ nanoparticles used for biodetection and evaluation of antioxidant behavior, Nanoscale 8 (2016) 5938–5945.
- [8] Y.Y. Li, X. He, J.J. Yin, Y.H. Ma, P. Zhang, J.Y. Li, Y.Y. Ding, J. Zhang, Y.L. Zhao, Z. F. Chai, Z.Y. Zhang, Acquired superoxide-scavenging ability of ceria nanoparticles, Angew. Chem. Int. Ed. 54 (2015) 1832–1835.
- [9] Q.Y. Liu, Q.Y. Jia, R.R. Zhu, Q.Q. Shao, D.M. Wang, P. Cui, J.C. Ge, 5,10,15,20-Tetrakis(4-carboxyl phenyl) porphyrin-CdS nanocomposites with intrinsic peroxidase-like activity for glucose colorimetric detection, Mater. Sci. Eng. C 42 (2014) 177–184.
- [10] D. Sun, X. Pang, Y. Cheng, J. Ming, S.J. Xiang, C. Zhang, P. Lv, C.C. Chu, X.L. Chen, G. Liu, N.F. Zheng, Ultrasound-switchable nanozyme augments sonodynamic therapy against multidrug-resistant bacterial infection, ACS Nano 14 (2020) 2063–2076.
- [11] X.X. Zheng, Q. Liu, C. Jing, Y. Li, D. Li, W.J. Luo, Y. Wen, Y. He, Q. Huang, Y. T. Long, C.H. Fan, Catalytic gold nanoparticles for nanoplasmonic detection of DNA hybridization, Angew. Chem. Int. Ed. 50 (2011) 11994–11998.
- [12] X.M. Shen, W.Q. Liu, X.J. Gao, Z.H. Lu, X.C. Wu, X.F. Gao, Mechanisms of oxidase and superoxide dismutation-like activities of gold, silver, platinum, and palladium, and their alloys: a general way to the activation of molecular oxygen, J. Am. Chem. Soc. 137 (2015) 15882–15891.
- [13] Y.H. Lin, J.S. Ren, X.G. Qu, Nano-gold as artificial enzymes: hidden talents, Adv. Mater. 26 (2014) 4200–4217.
- [14] L. Han, P. Liu, H.J. Zhang, F. Li, A.H. Liu, Phage capsid protein-directed MnO₂ nanosheets with peroxidase-like activity for spectrometric biosensing and evaluation of antioxidant behaviour, Chem. Commun. 53 (2017) 5216–5219.
- [15] B. Dutta, S. Biswas, V. Sharma, N.O. Savage, S.P. Alpay, S.L. Suib, Mesoporous manganese oxide catalyzed aerobic oxidative coupling of anilines to aromatic azo compounds, Angew. Chem. Int. Ed. 55 (2016) 2171–2175.
- [16] Y. Cao, X.D. Meng, D.D. Wang, K. Zhang, W.H. Dai, H.F. Dong, X.J. Zhang, Intelligent MnO₂/Cu_{2-x}S for multimode imaging diagnostic and advanced singlelaser irradiated photothermal/photodynamic therapy, ACS Appl. Mater. Interfaces 10 (2018) 17732–17741.
- [17] A.D. Balaev, N.V. Volkov, N.V. Sapronova, K.A. Sablina, A.D. Vasilyev, Magnetic properties of MnGeO₃ single crystals with orthorhombic structure, J. Phys. Condens. Matter 21 (2009) 336006.
- [18] Y.Y. Guo, L. Yan, R.Y. Zhang, H. Ren, A.H. Liu, CoO-supported ordered mesoporous carbon nanocomposite based nanozyme with peroxidase-like activity for colorimetric detection of glucose, Process Biochem. 81 (2019) 92–98.
- [19] H. Ren, L. Yan, M.J. Liu, Y.B. Wang, X. Liu, C.Y. Liu, K. Liu, L.X. Zeng, A.H. Liu, Green tide biomass templated synthesis of molybdenum oxide nanorods supported on carbon as efficient nanozyme for sensitive glucose colorimetric assay, Sens. Actuators, B 296 (2019) 126517.
- [20] D.D. Wang, H.H. Wu, S.Z.F. Phua, G.B. Yang, W.Q. Lim, L. Gu, C. Qian, H.B. Wang, Z. Guo, H.Z. Chen, Y.L. Zhao, Self-assembled single-atom nanozyme for enhanced photodynamic therapy treatment of tumor, Nat. Commun. 11 (2020) 357.
- [21] Y. Wu, L. Jiao, X. Luo, W.Q. Xu, X.Q. Wei, H.J. Wang, H.Y. Yan, W.L. Gu, B.Z. Xu, D. Du, Y.H. Lin, C.Z. Zhu, Oxidase-like Fe-N-C single-atom nanozymes for the detection of acetylcholinesterase activity, Small 15 (2019) 1903108.
- [22] H.J. Xiang, W. Feng, Y. Chen, Single-atom catalysts in catalytic biomedicine, Adv. Mater. 32 (2020) 1905994.
- [23] M.H. Li, J.X. Chen, W.W. Wu, Y.X. Fang, S.J. Dong, Oxidase-like MOF-818 nanozyme with high specificity for catalysis of catechol oxidation, J. Am. Chem. Soc. 142 (2020) 15569–15574.
- [24] H.Z. Fan, Y.Y. Li, J.B. Liu, R. Cai, X.S. Gao, H. Zhang, Y.L. Ji, G.J. Nie, X.C. Wu, Plasmon-enhanced oxidase-like activity and cellular effect of Pd-coated gold nanorods, ACS Appl. Mater. Interfaces 11 (2019) 45416–45426.

- [25] H.K. Yang, J.Y. Xiao, L. Su, T. Feng, Q.Y. Lv, X.J. Zhang, Oxidase-mimicking activity of the nitrogen-doped Fe₃C@C composites, Chem. Commun. 53 (2017) 3882–3885.
- [26] X. Huang, F. Xia, Z.D. Nan, Fabrication of FeS₂/SiO₂ double mesoporous hollow spheres as an artificial peroxidase and rapid determination of H₂O₂ and glutathione, ACS Appl. Mater. Interfaces 12 (2020) 46539–46548.
- [27] X. Liu, L. Yan, H. Ren, Y.Y. Cai, C.Y. Liu, L.X. Zeng, J. Guo, A.H. Liu, Facile synthesis of magnetic hierarchical flower-like Co₃O₄ spheres: mechanism, excellent tetra-enzyme mimics and their colorimetric biosensing applications, Biosens. Bioelectron. 165 (2020) 112342.
- [28] X. Liang, L. Han, White peroxidase-mimicking nanozymes: colorimetric pesticide assay without interferences of O-2 and color, Adv. Funct. Mater. 30 (2020) 2001933
- [29] T. Pirmohamed, J.M. Dowding, S. Singh, B. Wasserman, E. Heckert, A.S. Karakoti, J.E.S. King, S. Seal, W.T. Self, Nanoceria exhibit redox state-dependent catalase mimetic activity, Chem. Commun. 46 (2010) 2736–2738.
- [30] S.S. Li, L. Shang, B.L. Xu, S.H. Wang, K. Gu, Q.Y. Wu, Y. Sun, Q.H. Zhang, H. L. Yang, F.R. Zhang, L. Gu, T.R. Zhang, H.Y. Liu, A nanozyme with photo-enhanced dual enzyme-like activities for deep pancreatic cancer therapy, Angew. Chem. Int. Ed. 58 (2019) 12624–12631.
- [31] W.Y. Zhen, Y. Liu, L. Lin, J. Bai, X.D. Jia, H.Y. Tian, X. Jiang, BSA-IrO₂: catalase-like nanoparticles with high photothermal conversion efficiency and a high X-ray absorption coefficient for anti-inflammation and antitumor theranostics, Angew. Chem. Int. Ed. 57 (2018) 10309–10313.
- [32] J.P. Chen, S. Patil, S. Seal, J.F. McGinnis, Rare earth nanoparticles prevent retinal degeneration induced by intracellular peroxides, Nat. Nanotechnol. 1 (2006) 142–150
- [33] Y.F. Zhou, C. Liu, Y. Yu, M. Yin, J.L. Sun, J. Huang, N. Chen, H. Wang, C.H. Fan, H. Y. Song, An organelle-specific nanozyme for diabetes care in genetically or diet-induced models, Adv. Mater. 32 (2020) 2003708.
- [34] P. Zhang, D. Sun, A. Cho, S. Weon, S. Lee, J. Lee, J.W. Han, D.P. Kim, W. Choi, Modified carbon nitride nanozyme as bifunctional glucose oxidase-peroxidase for metal-free bioinspired cascade photocatalysis, Nat. Commun. 10 (2019) 940.
- [35] Y. Liu, J.J. Du, M. Yan, M.Y. Lau, J. Hu, H. Han, O.O. Yang, S. Liang, W. Wei, H. Wang, J.M. Li, X.Y. Zhu, L.Q. Shi, W. Chen, C. Ji, Y.F. Lu, Biomimetic enzyme nanocomplexes and their use as antidotes and preventive measures for alcohol intoxication, Nat. Nanotechnol. 8 (2013) 187–192.
- [36] X. Hai, Y.W. Li, K.X. Yu, S.Z. Yue, Y.F. Li, W.L. Song, S. Bi, X.J. Zhang, Synergistic in-situ growth of silver nanoparticles with nanozyme activity for dual-mode biosensing and cancer theranostics, Chin. Chem. Lett. 32 (2021) 1215–1219.
- [37] K.L. Fan, J.Q. Xi, L. Fan, P.X. Wang, C.H. Zhu, Y. Tang, X.D. Xu, M.M. Liang, B. Jiang, X.Y. Yan, L.Z. Gao, In vivo guiding nitrogen-doped carbon nanozyme for tumor catalytic therapy, Nat. Commun. 9 (2018) 1440.
- [38] Y.Y. Huang, Z. Liu, C.Q. Liu, E.G. Ju, Y. Zhang, J.S. Ren, X.G. Qu, Self-assembly of multi-nanozymes to mimic an intracellular antioxidant defense system, Angew. Chem. Int. Ed. 55 (2016) 6646–6650.
- [39] J.X. Wu, Y.J. Yu, Y. Cheng, C.Q. Cheng, Y.H. Zhang, B. Jiang, X.Z. Zhao, L.Y. Miao, H. Wei, Ligand-dependent activity engineering of glutathione peroxidasemimicking MIL-47(V) metal-organic framework nanozyme for therapy, Angew. Chem. Int. Ed. 60 (2021) 1227–1234.
- [40] X.X. Xi, X. Peng, C.Y. Xiong, D.Y. Shi, J.L. Zhu, W. Wen, X.H. Zhang, S.F. Wang, Iron doped graphitic carbon nitride with peroxidase like activity for colorimetric detection of sarcosine and hydrogen peroxide, Microchim. Acta 187 (2020) 383.
- [41] Q.Y. Liu, Y.T. Yang, H. Li, R.R. Zhu, Q. Shao, S.G. Yang, J.J. Xu, NiO nanoparticles modified with 5,10,15,20-tetrakis(4-carboxyl pheyl)-porphyrin: promising peroxidase mimetics for H₂O₂ and glucose detection, Biosens. Bioelectron. 64 (2015) 147–153.
- [42] S.B. He, A.L. Hu, Q.Q. Zhuang, H.P. Peng, H.H. Deng, W. Chen, G.L. Hong, Ascorbate oxidase mimetic activity of copper(II) oxide nanoparticles, Chembiochem 21 (2020) 978–984.
- [43] S.B. He, P. Balasubramanian, A.L. Hu, X.Q. Zheng, M.T. Lin, M.X. Xiao, H.P. Peng, H.H. Deng, W. Chen, One-pot cascade catalysis at neutral pH driven by CuO tandem nanozyme for ascorbic acid and alkaline phosphatase detection, Sens. Actuators, B 321 (2020) 128511.
- [44] L. Han, H.J. Zhang, D.Y. Chen, F. Li, Protein-directed metal oxide nanoflakes with tandem enzyme-Like characteristics: colorimetric glucose sensing based on one-Pot enzyme-free cascade catalysis, Adv. Funct. Mater. 28 (2018) 1800018.
- [45] H.L. Wang, Z.W. Xu, Z. Li, K. Cui, J. Ding, A. Kohandehghan, X.H. Tan, B.C. Zahiri, B.C. Olsen, C.M.B. Holt, D. Mitlin, Hybrid device employing three-dimensional arrays of MnO in carbon nanosheets bridges battery-supercapacitor divide, Nano Lett. 14 (2014) 1987–1994.
- [46] Y.T. Chu, L.Y. Guo, B.J. Xi, Z.Y. Feng, F.F. Wu, Y. Lin, J.C. Liu, D. Sun, J.K. Feng, Y. T. Qian, S.L. Xiong, Embedding MnO@Mn₃O₄ nanoparticles in an N-doped-carbon framework derived from Mn-organic clusters for efficient lithium storage, Adv. Mater. 30 (2018) 1704244.